

Measuring atmospheric turbulence strength based on differential imaging of light column

Honghua Huang (黄宏华)*, Chaolong Cui (崔朝龙), Wenyue Zhu (朱文越), Zaihong Hou (侯再红), Yi Wu (吴毅), and Ruizhong Rao (饶瑞中)

Key Laboratory of Atmospheric Composition and Optical Radiation of Chinese Academy of Sciences, Anhui Institute of Optics and Fine Mechanics, Chinese Academy of Sciences, Hefei 230031, China

*Corresponding author: hhuang@aiofm.ac.cn

Received August 24, 2013; accepted November 5, 2013; posted online December 9, 2013

We propose and experimentally evaluate a novel approach to measure atmospheric turbulence, in which imaging of light column technology is integrated into a differential motion method. In the approach, a large acquisition scene of the light column and a narrow field of view of one pixel of the charge-coupled device respectively allow high temporal and spatial resolutions, which offer the possibility of path-integrated turbulence strength measurement with multiple paths. In addition, we describe the measurement principle of the approach. Lastly, comparative experiment is performed to verify the feasibility of the approach.

OCIS codes: 010.0010, 010.3640, 120.0280, 010.1330.

doi: 10.3788/COL201311.120101.

Atmospheric turbulence leads to serious problems in optical engineering applications. When a light beam propagates in a turbulent atmosphere, its wave front will be distorted and the beam pattern will also be altered, thus resulting in beam wander and intensity fluctuation (scintillation). In astronomical observations, the performance of a telescope is highly dependent on the strength of atmospheric turbulence^[1]. Several optical parameters characterize atmospheric turbulence. The atmospheric coherence length r_0 is a key parameter that describes the path-integrated turbulence from the light source to the receiver plane of the instrument. Adaptive optics design depends on this parameter. Surveying sites for large astronomical telescopes and evaluating the performance of optical systems also depend on this parameter. Numerous techniques have been developed to measure r_0 . The differential image motion monitor (DIMM) method is widely accepted and typically used to measure r_0 in astronomy. r_0 is determined by the refractive index structure constant C_n^2 on the path profile, and thus, it can be obtained by turbulence strength profiling methods, such as multi-aperture scintillation sensor, scintillation detection and ranging, lunar scintillometer, and slope detection and ranging^[2–5]. However, these techniques and numerous other optical methods are used only at night under clear sky conditions because stars or the moon are used as light source. To date, numerous active measuring methods based on lidar techniques to detect atmospheric turbulence have been proposed. These methods are mainly based on turbulence-induced residual scintillation of lidar signals, enhanced backscattering, and image motion of secondary sources produced by laser beams^[6]. The method based on laser signal scintillation suffers from laser energy fluctuations. Moreover, its highest detection altitude is limited by laser energy and signal-to-noise ratio (SNR). The method based on laser beam motion suffers from a round-trip path i.e., the optical wave propagates through the turbulent medium twice. The image motion received by the image plane includes the random motion of the transmitted beam and

the motion of reflected beam. Thus, r_0 is difficult to be obtained based on these methods. Recently, Belen'kii *et al.* proposed the differential image motion lidar to measure vertical profiles; this method can overcome the round-trip path, vibration, laser instability, and other unstable factors^[7]. Thus, r_0 can be obtained by probing the atmosphere sequentially at different points along the optical path.

In this letter, we propose a new atmospheric turbulence measurement approach in which light column imaging technology is combined with the DIMM method. Through two scans, the laser beam can be imaged from a distance of several hundred meters to several kilometers. Thus, temporal resolution is increased. The spatial resolution of images ranges from several meters to several hundred meters, thereby providing an option to choose images from different altitudes. We can also use the images to calculate the path-integrated turbulence strength r_0 with various paths. Furthermore, the DIMM approach can avoid the uplink propagation effect of the transmitted beam, thus indicating that the conventional DIMM method can measure turbulence strength in a particular optical path^[7,8].

The schematic of the system is shown in Fig. 1. The system consists of two parts: the laser emitting unit and the telescope receiving unit. L (baseline) is the distance between these units. A mask plate with two apertures is installed in front of the telescope, and two wedge prisms are installed on each aperture. When a pulsed laser beam is emitted toward the zenith direction, and the beam forms a light column, a trigger signal is sent to the charge-coupled device (CCD) of the telescope. Rays from the light column are refracted by the two wedge prisms in the aperture, thus forming two light column images on the CCD. The vertical pixels in the image correspond to the laser beam at different altitudes. The imaging altitude of the light beam in the CCD ranges from initial altitude h_0 to maximum altitude h_{\max} because of the limited field of view (FOV). If the beam at altitude z forms the pixel with FOV $d\theta$ and the distance between

the beam and the telescope is R from the telescope, then the energy received at the pixel can be calculated as^[9–11]

$$E_r = K_1 E_0 A \frac{\beta_N(z, \theta) T_z T_R dz}{R^2}, \quad (1)$$

where K_1 is a calibration constant that represents the optical efficiency of the system, E_0 is the single pulsed laser energy, θ is the scattering angle of the air molecules and the aerosols, A is the effective collecting area of the optics, T_z and T_R are respectively the total atmospheric transmittance from the laser to altitude z and from altitude z along the slant path R to the telescope, $\beta_N(z, \theta)$ is the scattering coefficient of the aerosol and the air molecules, and dz is the length of the imaged beam on one pixel.

According to the geometric relationship shown in Fig. 1, height z is given by

$$z = -L / \tan \theta. \quad (2)$$

Through differentiation, Eq. (2) is transformed into the following form:

$$\begin{aligned} dz &= -L(-\sec^2 \theta d\theta / \tan^2 \theta) \\ &= L d\theta / (L^2 / R^2) = R^2 d\theta / L. \end{aligned} \quad (3)$$

Thus, Eq. (1) is transformed into the following form:

$$E_r = K_1 E_0 A \beta_N(z, \theta) T_z T_R d\theta / L. \quad (4)$$

According to Eq. (3), the spatial resolution of the image depends on baseline L , the FOV of one pixel, and slant distance R . Moreover, this resolution increases with R . According to Eq. (4), the received signal intensity of the proposed approach does not depend on the $1/R^2$ unlike the received signal intensity of traditional lidar.

As shown in Fig. 1, if the baseline and FOV of the CCD are determined and the laser beam altitude corresponding to the pixel at the bottom or top of the beam image in the CCD is known, then we can individually calculate the laser beam altitude corresponding to other pixels in the beam image of the CCD. Based on the known FOV of the CCD, if the baseline is small and the initial altitude is low, then an image with high resolution can be realized

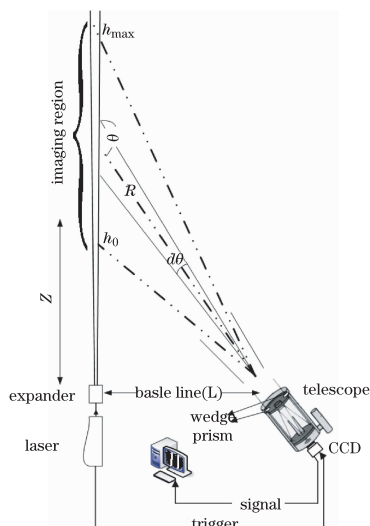


Fig. 1. Schematic of the measurement system.

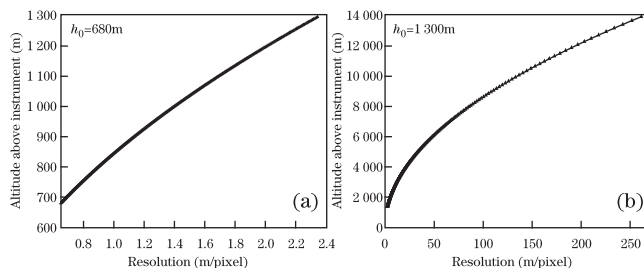


Fig. 2. Altitude resolution. (a) Initial altitude $h_0 = 680$ m and (b) initial altitude $h_0 = 1300$ m.

in the lowest levels. By contrast, if the initial altitude is high, then the highest detection altitude can be realized. From the focal length of the telescope and the pixel size of the CCD camera, the FOV of one pixel of the CCD can be determined. From the baseline and the initial altitude, the altitude of the laser beam corresponding to each pixel can be obtained. For example, the following parameters are known: baseline distance of 2 m, 658×496 (pixels), the pixel size of the CCD camera is of $10 \mu\text{m}$, and the focal length of the telescope is 3.56 m. If the initial altitude is assumed to be 680 m, then the maximum detection altitude is 1300 m and the altitude resolution is less than 3 m. If the initial altitude is assumed to be 1300 m, then the maximum detection altitude is 14000 m and the altitude resolution of the image is between 2 and 250 m. Spatial resolution, as a function of altitude, is shown in Fig. 2. Within the detection range of 680 m to 14 km, the initial altitude angle can only be changed once to guarantee that the laser image has good temporal and spatial resolution.

Aside from the system parameters, which include single-pulsed laser energy, optical efficiency, collecting area of the receiver, distance of baseline, and FOV of one pixel, the atmospheric condition also has an important influence on the received signal intensity of one pixel. The influence of the atmosphere on the received signal intensity involves atmospheric transmittance T_z , T_R , and the scattering coefficient $\beta_N(z, \theta)$. The following signal intensity is calculated for an average continental (Hefei, China) atmospheric model and a rural aerosol model (vis = 23 km)^[12]. The most intense pixel of the CCD corresponds to the beam image at 1.3 km, and the weakest pixel corresponds to the beam image at 14 km. Then, we obtain the intensity ratio of the two pixels as

$$\begin{aligned} &\beta_N(1.3 \text{ km}, \theta) T_{Z1.3 \text{ km}} T_{R1.3 \text{ km}} / \beta_N(14 \text{ km}, \theta) \\ &\cdot T_{Z14 \text{ km}} T_{R14 \text{ km}} = 52. \end{aligned} \quad (5)$$

According to Eq. (5), the intensity difference between the two pixels is as large as 52 times, and pixel intensity on the CCD is decreased with increasing beam altitude. Therefore, atmospheric condition has a significant influence on the received signal strength.

Random fluctuation of the atmospheric refractive index leads to beam wander. For the round-trip path shown in Fig. 1, the beam wander can be characterized statistically by the image centroid displacement at the target plane. The differential image motion displacement φ_d may be calculated as^[7]

$$\begin{aligned} \varphi_d &= \varphi_{1A} - \varphi_{2A} = (\varphi_{LB} - \varphi_{1,S}) - (\varphi_{LB} - \varphi_{2,S}) \\ &= \varphi_{2,S} - \varphi_{1,S}, \end{aligned} \quad (6)$$

Table 1. System Specifications

Feature	Specification
Laser	QUANTEL Brilliant-B
Wavelength (nm)	532
Pulse Repetition Frequency (Hz)	20
Pulse Energy (mJ)	180
Telescope	Meade 14-inch
Focal Length (m)	3.56
Aperture Diameter (mm)	100
Center Distance of Apertures (mm)	250
CCD	Andor luca-S
Active Pixel	658×496
Pixel Size (μm)	10.0×10.0
DAC Output (bits)	14
Exposure Time (ms)	0.47
Frame Rate (s^{-1})	37 frames
Baseline (m)	6

where φ_{1A} and φ_{2A} are the centroid positions of the two images, φ_{LB} is the displacement caused by the wave front tilt of the transmitted beam, and $\varphi_{1,S}$ and $\varphi_{2,S}$ are the displacements caused by the wave front tilts of the reflected wave in the two receiving apertures. In this manner, the DIMM method eliminates random motion of the transmitted beam. The differential image motion variance is given by

$$\sigma_d^2 = \langle \varphi_d^2 \rangle = \langle (\varphi_{2,S} - \varphi_{1,S})^2 \rangle. \quad (7)$$

In the vertical direction, adjacent image displacements overlap with each other because of turbulence. Thus, we cannot calculate beam wander at a certain altitude in the vertical direction. In the horizontal direction, a certain pixel corresponds to the image of the beam at a certain altitude. Moreover, turbulence leads to beam wander in the horizontal direction. Thus, we can obtain turbulence strength on the optical path from the beam to the receiver by determining the differential wander statistics of the two beams on their images in the horizontal direction. The variance σ_1^2 of the differential longitudinal motion is given by^[8]

$$\sigma_1^2 = 2\lambda^2 r_0^{-5/3} [0.179D^{-1/3} - 0.0968d^{-1/3}], \quad (8)$$

where D is the diameter of the apertures through which the tilts are measured, and d is the center distance of the two apertures. The beam centroid displacements are related to the turbulence on the entire path.

A turbulence lidar based on differential imaging of light column has been developed based on the aforementioned theories. The lidar is composed of a pulsed laser, a telescope, and a CCD. The specifications of the system are listed in Table 1.

Experiments were performed on the night of March 15, 2013 in Hefei, China. The sky was filled with thin and high clouds, which were suitable for the altitude calibration of the pixel in the image. Cloud height was determined as 10 km by a Mie lidar. The image of the

laser beam and the clouds is shown in Fig. 3(a). We kept the image of the clouds out of the CCD target plane by changing the altitude angle of the telescope. The image of the laser beam is shown in Fig. 3(b).

According to the system parameters listed in Table 1, the initial altitude of the light column in the image was 3.108 km if the maximum altitude of the light column in the CCD image was 10.039 km. The altitude resolution of each pixel ranged from 4 to 46 m, as shown in Fig. 4(a). In the vertical direction, the cloud image had 20 pixels in the CCD target plane and the cloud height in the image was approximately 760 m, according to Fig. 4(a). Based on cloud height, the image of the clouds moved out of the CCD target plane when the altitude angle of the telescope was changed. Thus, the altitude of the laser beam corresponding to the pixel on top of the CCD image below the cloud was 9.279 km. According to the system parameters of our experiment system, the maximum altitude of the image was calculated to be 9.275 km if the initial altitude was 2.945 km. The altitude resolution of each pixel ranged from 4 to 40 m, as shown in Fig. 4(b). Based on the preceding analysis, we believe that the pixel at the bottom of the CCD beam image corresponds to the laser beam image at an altitude of 3 km, whereas the pixel on top of the CCD beam image corresponds to the laser beam image at an altitude of 9 km. According to the altitude resolution of each pixel, the pixel position corresponding to the light column of the pixel at the 5-km path could be determined. A conventional DIMM instrument that uses a star as a light source was used to measure r_0 of the entire layer. The DIMM system was 100 m away from the turbulence lidar, and the altitude difference of the two instruments was 8 m. According to Eqs. (6) and (7), as well as the system parameters in Table 1, image displacements in the horizontal direction corresponding to the light columns at 3, 5, and 9-km altitudes could be obtained. The atmospheric coherence length r_0 at the three altitudes could be obtained by Eq. (8) through the statistics of differential motion variances of the image displacements. Similarly, the entire layer of r_0 could be obtained by the DIMM instrument through the statistics of differential motion variances of the star. The measured atmospheric coherence length r_0 is shown in Fig. 5. DIMM data during the period from 2130 to 2150 were not obtained because the star was blocked by the high clouds.

According to the measurement results of optical turbulence in the atmosphere, the atmospheric turbulence in the boundary layer was stronger than that in the free atmosphere. The proposed r_0 measurement approach based on the statistics of the wave front tilt fluctuation

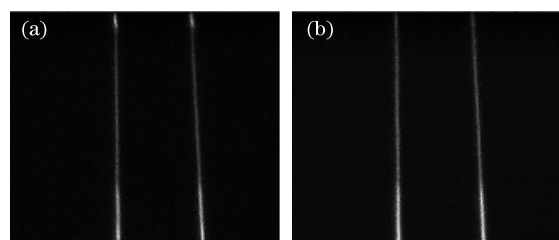


Fig. 3. Laser beam image. Images of the light column (a) with cloud and (b) without cloud.

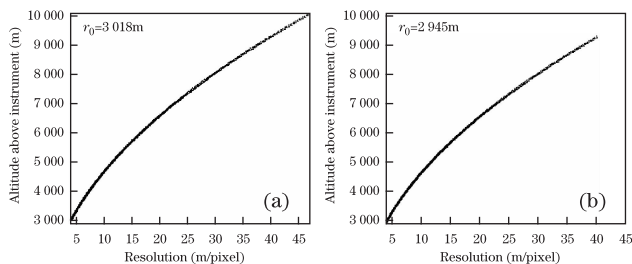


Fig. 4. Altitude resolution. (a) Initial altitude $h_0 = 3018$ m and (b) initial altitude $h_0 = 2945$ m.

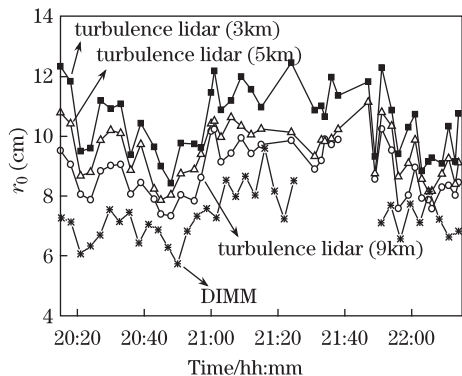


Fig. 5. Experimental result. The line with squares is the result of the 3-km path. The line with triangles is the result of the 5-km path. The line with circles is the result of the 9-km path. The line with stars is the result of the entire atmosphere.

is extremely sensitive to the turbulence in the boundary layer. Moreover, r_0 varies with the path-integrated turbulence. Figure 5 shows the r_0 results for the 3, 5, and 9-km turbulence obtained by the turbulence lidar based on the differential imaging of light column. According to the measurement results, the correlation coefficient was 91.4% between the results of 3 and 5 km, 91.3% between 5 and 9 km, and 87.1% between 3 and 9 km. The results for the entire layer were obtained with another DIMM instrument that uses a star as a light source. The correlation coefficient between the 9-km turbulence and the entire layer was 60.9% because of the difference between the integrated path and the measurement sites. These three groups of data exhibit better correlation with each other. The results measured with turbulence lidar demonstrate the same trend as the results obtained by conventional methods. In addition, r_0 decreased with increasing path length. The aforementioned measurement results are consistent with common experimental results. The correlation results at the three altitudes and the comparison trend with the results obtained via mature instruments verified the feasibility of the proposed approach.

However, this approach exhibits a measurement error because of limitations in the measurement technique. Therefore, measurement accuracy should be considered. Although the proposed approach is based on the DIMM method, several differences can be observed. As shown in Eq. (8), the differential variance depends on altitude, path-integrated turbulence, sub-aperture diameter, and sub-aperture separation. In the DIMM method, calculation is based on the positions of an image in the focal plane, and thus, position calculation is related to the im-

age centroid. However, even if the pair of images being measured by the DIMM method is completely steady, the motion of the measured image is still not zero because the coordinates of the images have several errors. Noise variances are added to the motion variance of the atmospheric image, thus influencing the accuracy of r_0 measurement. Sariazin *et al.* showed that accuracy is influenced by three types of errors: instrumental noise, statistical error, and exposure time error^[8,13]. In statistical error, the parameter r_0 is a known ensemble quantity that describes the average strength of the Kolmogorov model of turbulence^[14]. Therefore, atmospheric turbulence should be stationary during the measurement period and samples should be statistically independent. In most observations, however, the differential variance of arrival-angle fluctuation is measured within a finite period, and the variance of image motion is obtained from N short-exposure images, thus leading to statistical error. The statistical error of differential variance is given by^[8]

$$\frac{\delta\sigma^2}{\sigma^2} = \sqrt{\frac{2}{N-1}}, \quad (9)$$

where N is the number of samples.

Based on the measurements of optical turbulence in the atmosphere, 10 min is regarded as the maximum time during which the atmosphere can be assumed to be constant^[15]. According to the results shown in Fig. 2, the initial altitude angle must be switched only once to detect the atmospheric turbulence from 680 to 14,000 m. Laser pulse repetition frequency is 20 Hz. For each initial altitude, a 2 min sample time corresponds to 2400 image frames, and 4 min is needed to obtain the images. Spare time is allowed for the change in initial altitude. Based on Eq. (9), a root-mean-square (RMS) uncertainty of 3% is obtained for 2400 image frames.

According to DIMM theory, image motion is assumed to be measured within, and thus, infinitely short exposures that are considered as sampling spots are completely “frozen” during exposure. This requirement limits exposure time to a relatively short value^[16]. In practice, satisfying this assumption is difficult because of high wind speed. In determining atmospheric turbulence strength based on DIMM measurements, exposure time should be restricted to 2 ms. Exposure time error is less than 5% if exposure time is approximately 1 ms^[17]. Exposure time error can be controlled by shortening exposure time. If the light source is a star or a continuous-wave laser, then image brightness increases with exposure time. For pulse-echo imaging, exposure time depends on maximum detection altitude and the velocity of light. Therefore, increasing exposure time is not necessary. By contrast, background noise increases with exposure time. The relationship between detection altitude and exposure time is given by

$$\Delta z = ct_p/2, \quad (10)$$

where Δz is the expected detection altitude, and t_p is the exposure time of the CCD. For example, if the maximum detection altitude is 15 km, then an exposure time of 0.1 ms is required. In the present experiment, the minimal exposure time of the experiment system was 0.47 ms because of the limitation of the CCD. Therefore, exposure time error can be controlled by shortening CCD exposure

time. In the proposed approach, the requirement for exposure time error is not strict.

Moreover, instrument error is the most important factor for the three types of errors in this approach. Calculating the image centroid depends on image size, the number of received laser photoelectrons, the background photoelectron quantity in the sky, and the read-out noise electrons of the CCD^[18]. According to Eq. (7), the received signal intensity a pixel decreases with increasing beam altitude because of the influence of atmospheric conditions. Therefore, high image quality is important. However, the current system is not optimal and requires further improvement. For example, in the imaging altitude of light columns ranging from 3 to 9 km based on the relationship among object distance, focal length, and image distance, if the focal length is constant, then image distance should change with object distance. By contrast, if image distance is fixed within the imaging range, then certain positions in the image may be obscure. In the present study, the image distance is fixed and the image quality is poor. In the future, finding the balanced point between initial and maximum measurement altitudes to obtain high image quality is necessary. In addition, the amount of photoelectrons received by the laser at the high altitude is less than the amount of photoelectrons at the bottom altitude. The SNR at high altitudes can be increased by decreasing altitude resolution, such as by binning operation. The brightness of an image increases with increasing laser energy. Furthermore, the altitude calibration used in this study is completed by a Mie lidar and related calculations. In this approach, if no cloud with appropriate altitude or no Mie lidar is available nearby to measure cloud height, then completing the calibration will be difficult. In our next work, we can select an appropriate delay time for the CCD to obtain the initial altitude of a light column. The relationship between initial altitude and delay time is given by

$$z = ct_d/2, \quad (11)$$

where z is the initial altitude, and t_d is the delay time. The initial altitude of the light column can be obtained by controlling the size of t_d . For example, a delay time of 0.02 ms is required if the initial altitude is 3 km. The maximum detection altitude can be calculated by Eq. (10). Then, the light column altitude of each pixel can be obtained based on the FOV of each pixel. These issues require further research.

However, although we can obtain high-resolution laser images from 3 to 9 km, we cannot obtain a r_0 profile with high resolution. In most observations, the differential variance of the arrival angle is measured within a finite period of time, thus making it a random variable. Similarly, the r_0 calculated from the differential variance of the arrival angle is also a random variable. Therefore, the r_0 obtained by single measurement fluctuates around its ensemble value^[14]. If r_0 is measured with high altitude resolution, then the differences among r_0 values obtained between the paths from one row of pixels and the next will be extremely small. Moreover, the fluctuations of r_0 and the measurement errors may be larger than the difference in their values, thus leading to errors and unphysical results. For example, r_0 decreases with

increasing path length, but errors cause r_0 obtained by the long path to be larger than r_0 obtained by the short path. The high vertical resolution of the laser image has potential advantages that are convenient for selecting expected altitudes according to the requirements of the experiment.

In conclusion, A new approach to measure turbulence strength is proposed. This approach can be considered as a hybrid of two commonly used atmospheric characteristic measurement techniques: the DIMM, in which light from a natural star is used to measure the integrated effect of atmospheric turbulence in terms of the atmospheric coherence parameter r_0 , and bistatic imaging lidar with a CCD camera, which can acquire image data from a large space range. To measure turbulence, the light column image with high spatial and temporal resolution provides an option to choose images with different altitudes, which can be used to calculate the turbulence strength parameter r_0 with various paths. The application of the DIMM method can avoid a round-trip path, vibration, laser instability, and other unstable factors that are common in most laser remote sensing technologies for turbulence strength. The feasibility of this approach is verified theoretically and experimentally.

This work was supported by the National Natural Science Foundation of China under Grant No. 41105020.

References

1. J. Mu, W. Zheng, M. Li, and C. Rao, *Chin. Opt. Lett.* **10**, 120101 (2012).
2. V. Kornilov, A. Tokovinin, O. Vozyakova, A. Zaitsev, N. Shatsky, S. Potanin, and M. Sarazin, *Proc. SPIE* **4839**, 837 (2003).
3. R. Avila, J. Vernin, and E. Masciadri, *Appl. Opt.* **36**, 7898 (1997).
4. A. Tokovinin, E. Bustos, and A. Berdja, *RAS, MNRAS* **404**, 1186 (2010).
5. R. W. Wilson, *RAS, MNRAS* **337**, 103 (2002).
6. A. Zilbermann and N. S. Kopeika, *J. Appl. Remote Sens.* **2**, 023540-1 (2008).
7. M. S. Belen'kii, D. W. Roberts, J. M. Stewart, and G. G. Gimmestad, *Opt. Lett.* **25**, 518 (2000).
8. M. Sarazin and F. Roddier, *Astron. Astrophys.* **227**, 294 (1990).
9. K. Meki, K. Yamaguchi, X. Li, Y. Sato, T. D. Kawahara, and A. Nomura, *Opt. Lett.* **21**, 1318 (1996).
10. J. E. Barnes, S. Bronner, R. Beck, and N. C. Parikh, *Appl. Opt.* **42**, 2647 (2003).
11. J. E. Barnes, N. C. Parikh Sharma, and T. B. Kaplan, *Appl. Opt.* **46**, 2922 (2007).
12. H. Wei, X. Chen, R. Rao, Y. Wang, and P. Yang, *Opt. Express* **15**, 8360 (2007).
13. A. Tokovinin, *PASP* **114**, 1156 (2002).
14. Z. Gong, J. Wang, and Y. Wu, *Appl. Opt.* **37**, 4541 (1998).
15. G. Gimmestad, D. Roberts, J. Stewart, and J. Wood, *Opt. Eng.* **51**, 101713(2012).
16. H. M. Martin, *PASP* **99**, 1360 (1987).
17. D. B. Soules, J. J. James, J. Drexler, and B. F. Draayer, *PASP* **108**, 817 (1996).
18. J. S. Morgan, D. C. Slanter, J. G. Timothy, and E. B. Jenkins, *Appl. Opt.* **28**, 1178 (1989).